SNX27-FERM-SNX1 complex structure rationalizes divergent trafficking pathways by SNX17 and SNX27

Xin Yong[a,1], Lin Zhao[a,1], Wenfeng Hu[a,1], Qingxiang Sun[b,1], Hyoungjun Ham[c,1], Zhe Liu[a,1], Jie Ren[d], Zhen Zhang[a], Yifei Zhou[a], Qin Yang[a], Xianming Mo[e], Junjie Hu[d], Daniel D. Billadeau[c,2], and Da Jia[a,2]

[a]Key Laboratory of Birth Defects and Related Diseases of Women and Children, Department of Paediatrics, West China Second University Hospital, State Key Laboratory of Biotherapy and Collaborative Innovation Center of Biotherapy, Sichuan University, Chengdu 610041, China; [b]Department of Pathology, State Key Laboratory of Biotherapy, West China Hospital, Sichuan University, Chengdu 610041, China; [c]Division of Oncology Research and Schulze Center for Novel Therapeutics, Mayo Clinic, Rochester, MN 55905; [d]Institute of Biophysics, Chinese Academy of Sciences, Beijing 100101, China; and [e]Department of Pediatric Surgery and Laboratory of Stem Cell Biology, State Key Laboratory of Biotherapy, West China Hospital, Sichuan University, Chengdu 610041, China

Edited by Gaya K. Amarasinghe, Washington University School of Medicine, St. Louis, MO, and accepted by Editorial Board Member Michael F. Summers June 29, 2021 (received for review March 23, 2021)

The molecular events that determine the recycling versus degradation fates of internalized membrane proteins remain poorly understood. Two of the three members of the SNX-FERM family, SNX17 and SNX31, utilize their FERM domain to mediate endocytic trafficking of cargo proteins harboring the NPxY/NxxY motif. In contrast, SNX27 does not recycle NPxY/NxxY-containing cargo but instead recycles cargo containing PDZ-binding motifs via its PDZ domain. The underlying mechanism governing this divergence in FERM domain binding is poorly understood. Here, we report that the FERM domain of SNX27 is functionally distinct from SNX17 and interacts with a novel DLF motif localized within the N terminus of SNX1/2 instead of the NPxY/NxxY motif in cargo proteins. The SNX27-FERM-SNX1 complex structure reveals that the DLF motif of SNX1 binds to a hydrophobic cave surrounded by positively charged residues on the surface of SNX27. The interaction between SNX27 and SNX1/2 is critical for efficient SNX27 recruitment to endosomes and endocytic recycling of multiple cargoes. Finally, we show that the interaction between SNX27 and SNX1/2 is critical for brain development in zebrafish. Altogether, our study solves a long-standing puzzle in the field and suggests that SNX27 and SNX17 mediate endocytic recycling through fundamentally distinct mechanisms.

membrane trafficking | endosome | endosomal sorting | sorting nexin | SNX27

Endosomes are key platforms for transmembrane receptor and lipid sorting as well as for cell signaling. Cell surface receptors arrive from endocytic or anterograde trafficking routes and are either sent to the lysosome for degradation or recycled to other compartments, including the plasma membrane and the trans-Golgi network (1–3). Endosomal trafficking is indispensable for maintaining plasma membrane homeostasis and is tightly regulated by many pivotal protein machineries (1–3). Consequently, dysregulation of this process contributes to the development of a variety of human diseases, including Parkinson's disease, Alzheimer's disease, and cancer (4–6). Finally, many intracellular pathogens, including vacuolar bacteria, human papilloma virus, and SARS-CoV-2, hijack the endosomal trafficking pathways for their infection and replication (7–10).

Members of the SNX-FERM subfamily have emerged as key proteins essential for sequence-dependent cargo recycling. The SNX-FERM subfamily is defined by the presence of a FERM domain, which interacts with NPxY/NxxY motifs located within the cytoplasmic tails of many transmembrane proteins, in addition to the phox homology (PX) domain, which is involved in phosphatidylinositol binding (2, 11) (Fig. 1*A*). The SNX-FERM subfamily encompasses three members: SNX17, SNX27, and SNX31 (2, 11). Unique to this subfamily, SNX27 also harbors a PDZ domain that can engage with PDZ-binding motifs (PDZbm) at the C-terminus of transmembrane proteins. SNX17 is a well-established regulator for endosomal trafficking and mediates trafficking of many cargoes bearing the NPxY/NxxY motif together with retriever (VPS35L, VPS26C, and VPS29), the CCC (COMMD/CCDC22/CCDC93) complex, and the actin-regulatory WASH complex (12–17). Established SNX17 cargoes include P-selectin, LDL receptor–related protein 1 (LRP1), VLDLR, and α5β1 integrins (12, 18–20). SNX31 is less studied; however, recent studies indicate that SNX31 can function analogously to SNX17 and regulate turnover and recycling of β1 integrin (21). In contrast with SNX17 and SNX31, SNX27 is most known to regulate endosomal trafficking of PDZbm-containing cargoes, such as glucose transporter GLUT1 and the β2 adrenergic receptor (22–24). SNX27 regulates endosomal trafficking through engaging with retromer (VPS35, VPS26A/B, and VPS29), a SNX–Bin/Amphiphysin/Rvs (BAR) dimer (SNX1/2 in complex with SNX5/6), and the WASH complex (23, 25–31). Both SNX17 and SNX27 have been linked with pathogenesis of multiple neurological disorders, such as Alzheimer's disease and Down's syndrome, emphasizing the importance of SNX-FERM–mediating endocytic recycling in development and human diseases (32–34). Interestingly, it was reported that the FERM domain of SNX27 could interact with peptides containing the NPxY/NxxY motif

Significance

The sorting nexin proteins are critical for endosomal trafficking and signaling. SNX17 and SNX27 are two SNX proteins displaying high similarity in domain structure, including a common FERM domain; however, they mediate distinct endocytic recycling pathways. We now solve this mystery by demonstrating that the FERM domains of SNX17 and SNX27 have different functions. Whereas the FERM domain of SNX17 recognizes the NPxY/NxxY motif, the same domain in SNX27 binds to a novel "DLF" motif within the N termini of SNX1/2. The interaction between SNX27 and SNX1/2 not only helps efficient retrieval of multiple cargoes but also promotes endosomal recruitment of SNX27. We further demonstrate that the SNX27–SNX1/2 interaction is crucial to neuronal growth and brain development in zebrafish.

Author contributions: D.D.B. and D.J. designed research; X.Y., L.Z., W.H., Q.S., H.H., Z.L., J.R., Z.Z., Y.Z., and Q.Y. performed research; X.M. and J.H. contributed new reagents/analytic tools; X.Y., L.Z., W.H., Q.S., H.H., Z.L., D.D.B., and D.J. analyzed data; and X.Y., D.D.B., and D.J. wrote the paper.

The authors declare no competing interest.

This article is a PNAS Direct Submission. G.K.A. is a guest editor invited by the Editorial Board.

See online for related content such as Commentaries.

[1]X.Y., L.Z., W.H., Q.S., H.H., and Z.L. contributed equally to this work.

[2]To whom correspondence may be addressed. Email: jiada@scu.edu.cn or billadeau.daniel@mayo.edu.

This article contains supporting information online at https://www.pnas.org/lookup/suppl/doi:10.1073/pnas.2105510118/-/DCSupplemental.

Published August 30, 2021.

(35, 36), yet unlike SNX17 and SNX31, SNX27 does not promote recycling of NPxY/NxxY motif-containing cargoes.

To investigate this paradox, we utilized a holistic approach, combining biochemical, structural, and cellular studies with in vivo animal models. We show that the FERM domains of the SNX-FERM family have distinct functions: whereas the FERM domain of SNX17 recognizes the NPxY/NxxY motif, the same domain in SNX27 specifically binds to a DLF motif located within the N terminus of SNX1/2. The interaction between SNX27 and SNX1/2 is necessary for not only the recruitment of SNX27 to endosomes but also the trafficking of membrane proteins, such as GLUT1 and TRAILR1. Finally, we show that interaction between SNX27 and SNX1/2 is critical for brain development in zebrafish, and the FERM domains of SNX17 and SNX27 are not interchangeable. Together, our data demonstrate that members of the SNX-FERM family regulate distinct endosomal trafficking routes via functionally divergent FERM domains and provide a unified answer for many different observations in the field.

Results

The N termini of SNX1/2 Harbor Multiple Copies of a Novel DLF Motif that Directly Interact with the FERM Domain of SNX27. Previous studies indicated that SNX27 associates with SNX1/2 through its FERM domain, but the regions of SNX1/2 responsible for the association remain undetermined (23). Both SNX1/2 and SNX5/6 belong to the SNX-BAR subfamily, which contain a BAR domain in addition to the conserved PX domain (Fig. 1*A*). SNX1/2 harbor an extra N-terminal region, which is predicted to be largely disordered and is absent in SNX5/6. To determine which region of SNX1/2 interacts with SNX27, we generated SNX1 fragments encoding the N terminus of SNX1 (SNX1-N) or deleting the N terminus (SNX1-ΔN). In both immunoprecipitation (IP) and glutathione S-transferase (GST) pull-down assays using purified proteins, we found that SNX1-N, but not SNX1-ΔN, interacted with the FERM domain of SNX27 (Fig. 1*B* and *SI Appendix*, Fig. S1*A*). Immunofluorescence staining revealed a strong colocalization between mCherry-SNX27 and YFP-SNX1, consistent with the notion that the two proteins function together to mediate endocytic recycling (Fig. 1 *C* and *D*). Although YFP-SNX1-N localized to the nucleus, a chimera construct fusing a nuclear export signal peptide KPI to the N terminus of SNX1-N (KPI-SNX1-N) displayed strong colocalization with mCherry-SNX27, consistent with the binding between SNX1-N and SNX27 (Fig. 1 *C* and *D*).

Sequence alignment of the N termini of SNX1 from *Homo sapiens*, *Danio rerio*, and *Drosophila melanogaster* and SNX2 from *H. sapiens* revealed a conserved motif that centered on three continuous residues, Asp-Leu-Phe or Asp-Ile-Phe, which we term the DLF motif (Fig. 1*E*). In the following discussion, the F89 of $SNX1^{68\text{-}90}$ or its equivalent was designated as position 0, and other residues were numbered with respect to this order (e.g., D87 was D_{-2}). Multiple lines of evidence suggested that the DLF motif could mediate the interaction with SNX27. First, $SNX1^{30\text{-}53}$ and $SNX1^{68\text{-}90}$, both of which contain one DLF motif, but not $SNX1^{90\text{-}140}$, which lacks a DLF motif, associated with the FERM domain of SNX27 in the GST pull-down and IP experiments (*SI Appendix*, Fig. S1 *B* and *C*). Second, $SNX2^{1\text{-}145}$ contains three DLF motifs, and fragments of SNX2-N encompassing each motif could bind SNX27 FERM domain (*SI Appendix*, Fig. S1 *C* and *D*). Finally, two fragments from the N termini of *D. melanogaster* SNX1 ($dmSNX^{1\text{-}53}$) and *D. rerio* SNX1 ($drSNX1^{83\text{-}98}$), which both contain one DLF motif, were also capable of interaction with SNX27 (*SI Appendix*, Fig. S1 *E*–*G*). Taken together, we identified a conserved novel motif localized at the N termini of SNX1/2, which mediates the interaction with SNX27 FERM.

Crystal Structure of the SNX27 FERM Domain in Complex with a SNX1 Peptide Encompassing the DLF Motif. In order to further understand the interaction mechanism between SNX1/2 and SNX27, we crystalized the SNX27 FERM domain in complex with multiple peptides derived from the N terminus of SNX1 or SNX2. A chimera construct encoding the SNX27 FERM domain fused with $SNX1^{78\text{-}90}$ yielded diffraction-quality crystals. The complex structure was solved by selenium single-wavelength anomalous diffraction (Se-SAD) and refined to a resolution of 1.95 Å (Fig. 2 *A*–*C* and *SI Appendix*, Fig. S2 and Table S1). Eight residues ($Q_{-6}E_{-5}P_{-4}Q_{-3}D_{-2}L_{-1}F_0A_1$) from SNX1 were observed in this crystal structure, which fit the omit map very well (*SI Appendix*, Fig. S3*A*). As the FERM domains of SNX27 and SNX17 are 24% identical at the amino acid level, the SNX27 FERM domain is highly similar to that of SNX17 (2.9 Å rmsd for all Cα atoms [Ca]) (35) and is comprised of three modules, F1, F2, and F3. Yet SNX27, different from SNX17 and SNX31, lacks the extended loop between β5C and β6C in the F3 module (Fig. 2 and *SI Appendix*, Fig. S2).

Despite the similarity in the overall structure, the SNX27 FERM domain differs from that of SNX17 in many details. Crystal structure of SNX17 in complex with the P-selection peptide reveals that the NPxY/NxxY cargo is accommodated by a hydrophobic groove formed by α1C and β5C in the F3 lobe of SNX17 (35) (Fig. 2 *D*–*F*). Specifically, SNX17 residues, including R319, L353, V380, and M384, recognize the core NPxY/NxxY sequence, whereas W321 of SNX17 binds the upstream hydrophobic residue $[I/V/F/Y]_{-5}$ (Fig. 2*F*). Unlike SNX17, the corresponding region of SNX27 contains numerous positively charged residues, suggesting that SNX27 might not bind the NPxY/NxxY sequence. Indeed, surface conservation analysis revealed that the NPxY/NxxY binding site was highly conserved among SNX17 homologs but was not conserved in SNX27 (*SI Appendix*, Fig. S3 *B*–*E*). For instance, the conserved L353 in SNX17 that is critical for recognizing the Y_0 residue of the core NPxY sequence is replaced with an alanine in SNX27 (A491) (*SI Appendix*, Fig. S2). Consistent with the importance of this residue in recognizing NPxY/NxxY-containing cargoes, we found that a wild-type (WT) SNX17 FERM domain, but not an L353A mutant, could interact with VLDLR, a member of the LDLR family that bears the NPxY motif and is a known SNX17 cargo protein (19, 37) (*SI Appendix*, Fig. S3*F*).

Adjacent to the NPxY/NxxY binding site, SNX27 and SNX17 display another major difference in the F3 module. SNX27 possesses a hydrophobic cavity, which is surrounded by positively charged residues that are used to accommodate the DLF motif from SNX1 (Fig. 2 *B* and *C*). Both the hydrophobic cave and surrounding positive residues are absent in the corresponding surface on SNX17, indicating that SNX17 may not interact with the DLF motif. Taken together, our structural analysis indicates that the FERM domains of SNX27 and SNX17, while adopting a similar overall fold, have different binding specificities resulting from unique amino acids at key positions within the F3 module required for NPxY/NxxY and DLF interaction.

Distinct Binding Preference of the FERM Domains of SNX27 and SNX17. In contrast with our structural analysis, previous studies showed that the FERM domain of SNX27 interacted with NPxY/NxxY-containing cargoes using peptide arrays (35, 36). To further investigate this, we compared the interaction of the SNX27 or SNX17 FERM domains with $SNX1^{68\text{-}90}$ or multiple NPxY/NxxY-containing proteins, including VLDLR, P-selectin, and LRP1 using GST pull-downs and isothermal titration calorimetry (ITC). The side-by-side comparison revealed that the SNX27 FERM domain specifically interacted with $SNX1^{68\text{-}90}$ WT but not the $SNX1^{68\text{-}90}$ DLF mutant ($D_{-2}L_{-1}F_0$/AAA) or VLDLR (Fig. 3*A*). In contrast, the SNX17 FERM domain was able to pull down VLDLR but not $SNX1^{68\text{-}90}$ WT (Fig. 3*B*). ITC assays revealed that the SNX27 FERM domain bound to $SNX1^{68\text{-}90}$ WT with a dissociation constant (K_d) of ~20 μM but did not bind to the NPxY/NxxY peptides derived from LRP1 and P-selectin (Fig. 3*C*). Conversely, the SNX17 FERM domain did not interact with $SNX1^{68\text{-}90}$ WT but selectively interacted with P-selectin

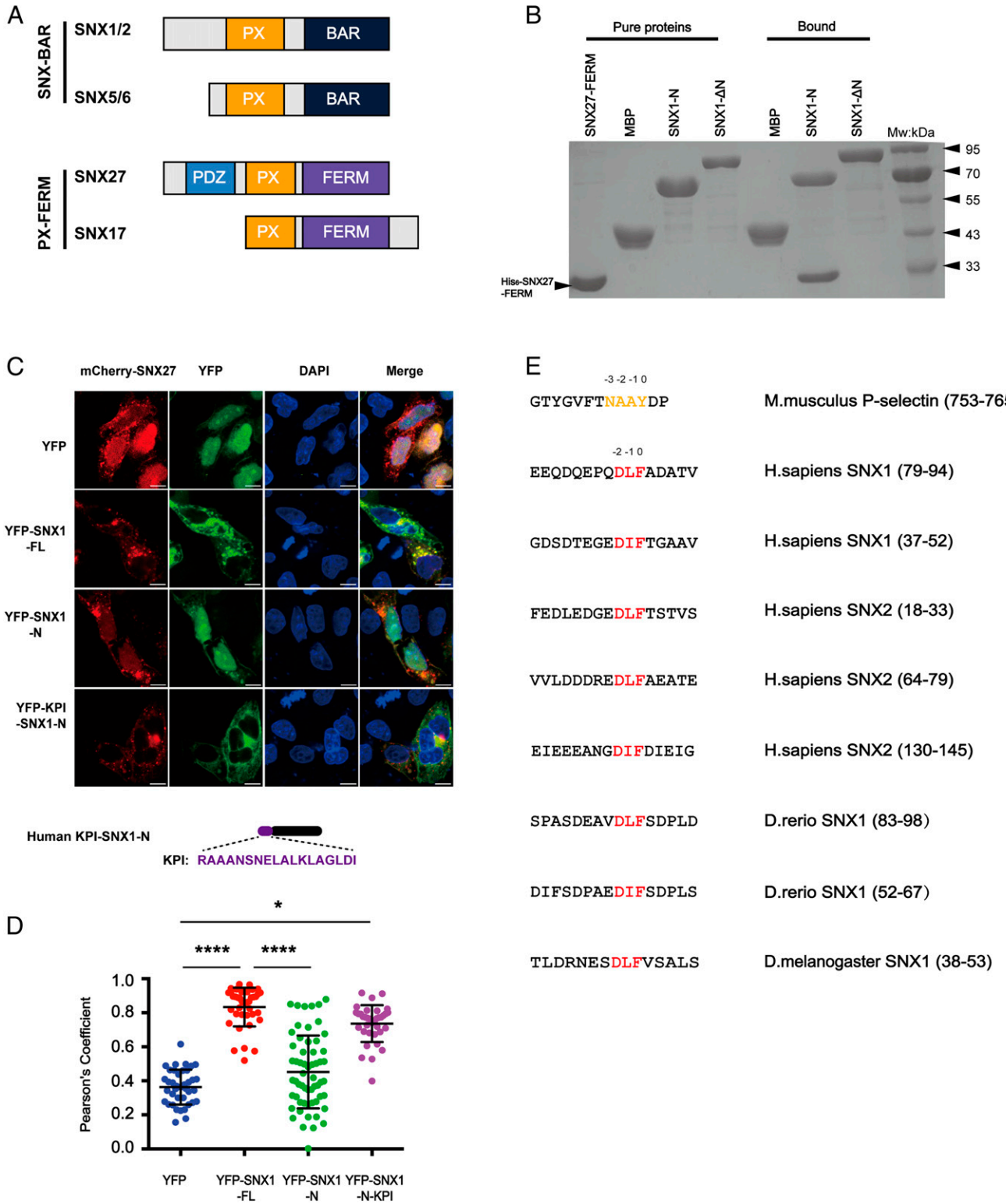

Fig. 1. SNX27 specifically binds to multiple motifs centered on DLF within the N termini of SNX1/2. (*A*) Domain architecture of SNX-BAR and SNX-FERM proteins used in this study. PX, BAR, FERM (band4.1-ezrin-radixin-moesin), and PDZ (postsynaptic density 95-discs large-zonula occludens). (*B*) MBP-SNX1-N, SNX1-ΔN, and MBP pull-down of purified His-tagged SNX27 FERM. Shown is a Coomassie Blue–stained sodium dodecyl sulphate–polyacrylamide gel electrophoresis (SDS/PAGE) gel with purified proteins (*Left*) and bound samples (*Right*). (*C*) Steady-state localization of different YFP-SNX1 constructs. HeLa cells were transiently transfected with mCherry-SNX27 (red) and YFP or YFP-SNX1 (green). A schematic diagram of KPI-SNX1-N is present on the bottom. (Scale bar: 10 μm.) (*D*) Colocalization of mCherry-SNX27 and YFP in cells in *C*. Each dot represents Pearson's correlation coefficients from one cell. Data were presented as mean ± SD, and *P* values were calculated using one-way ANOVA and Tukey's multiple comparisons test. $*P < 0.05$; $****P < 0.0001$. (*E*) Sequence alignment of multiple fragments from the N termini of SNX1 and SNX2 highlights a DLF motif. Red color indicates the conserved DLF or DIF residues. The NPxY/NxxY motif in P-selectin is colored in orange and used for comparison.

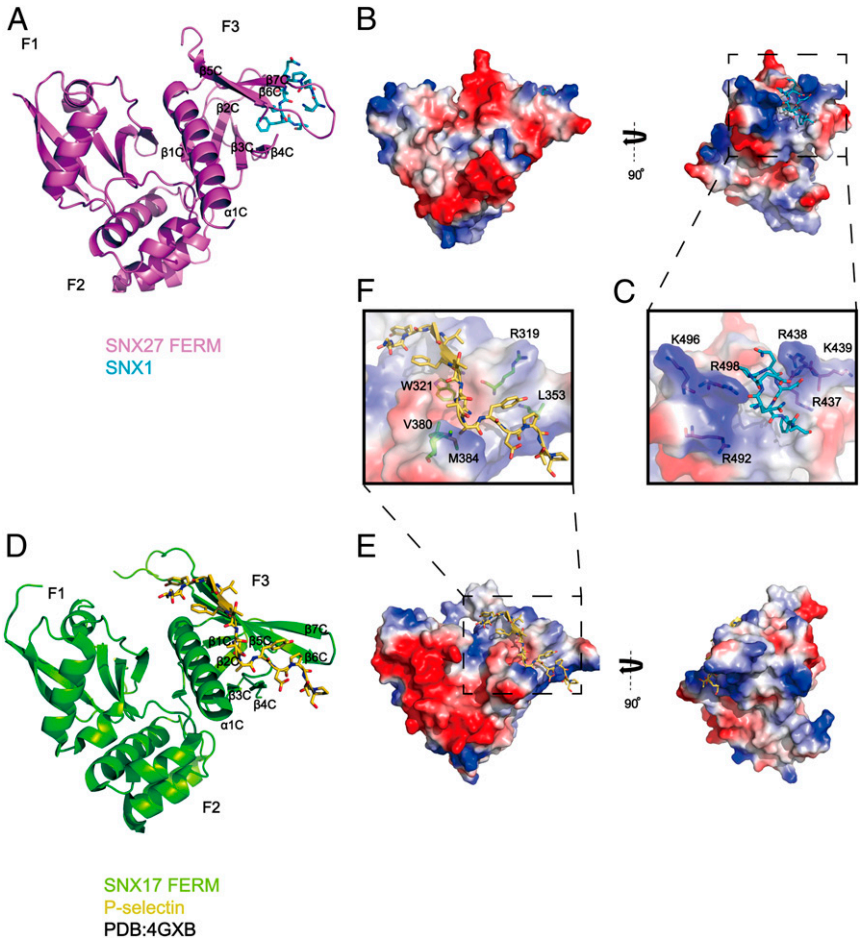

Fig. 2. Crystal structure of SNX27-FERM-SNX1 and its comparison with the SNX17-FERM-P-selectin structure. (*A*) Ribbon diagram of SNX27 FERM domain (violet) in complex with the SNX1 peptide, which is represented as cyan sticks. The three submodules of SNX27 FERM, F1, F2, and F3, are marked, and the secondary structure of F3 is labeled. (*B*) The overall structure is shown in two perpendicular views depicted by SNX27 surface colored for electrostatic potential, with $SNX1^{83-90}$ peptide colored in cyan. Red and dark blue colors indicate negatively or positively charged surfaces of SNX27 FERM, separately. White colors highlight the hydrophobic region on SNX27 FERM surface. (*C*) A close-up inset image of the interface in the dashed line box shown in *B*. SNX27 is represented as a partially transparent surface with specific positively charged side chains around the hydrophobic binding pocket in accommodation for SNX1. (*D*) SNX17 in complex with cargo P-selectin (Protein Data Bank: 4GXB) is depicted with analogous representations to those shown for SNX27 in *A*. (*E*) SNX17 in complex with cargo P-selectin is represented similarly to SNX27 shown in *B*. (*F*) A zoomed-in picture of the interface between SNX17 and P-selectin in the dashed line box shown in *E*. A partially transparent electrostatic surface potential map of SNX17 is presented. Critical residues involved in interacting with P-selectin are shown in stick mode.

and LRP1 peptides with a K_d of ~2.7 μM and 6 μM, respectively (Fig. 3*D*), which is in agreement with previous studies (35).

Prior work suggested that phosphorylation of the tyrosine within the NPxY/NxxY motif of APP might enhance its interaction with the SNX27 FERM (35). We therefore examined the interaction between SNX27 and phosphorylated (APP-p) or nonphosphorylated APP (*SI Appendix*, Fig. S4). APP bound to SNX17 much weaker than P-selectin and LRP1, with a K_d of ~80 μM (*SI Appendix*, Fig. S4*B*). However, we were still able to detect its interaction with SNX17. Interestingly, phosphorylation of the tyrosine (APP-p) completely abolished the interaction between SNX17 and APP (*SI Appendix*, Fig. S4*B*). In contrast, we did not detect an interaction between SNX27 and APP or APP-p in either GST pull-down or ITC assays (*SI Appendix*, Fig. S4). Collectively, our biochemical and structural data indicate that in contrast to the FERM domain of SNX17, the FERM domain of SNX27 does not interact with the NPxY/NxxY motif but instead interacts with DLF motifs found in the N termini of SNX1/2.

Mechanism of Recognition of the DLF Motif by the SNX27 FERM Domain. Our SNX27-FERM-SNX1 complex structure reveals that the SNX1 peptide binds to a highly conserved surface on the F3 module of the SNX27 FERM domain (Fig. 4*A*). The SNX1 peptide forms a hairpin structure and binds to a groove formed by β4C, β7C, and an extended loop between β1C and β2C of SNX27. The interactions involve multiple salt bridges and hydrogen bonds as well as Van der Waal forces, resulting in burying a solvent accessible surface area of 980 $Å^2$ as calculated by the PISA server (https://www.ebi.ac.uk) (38). The side chains of F_0 and L_{-1} are deeply inserted in a hydrophobic pocket formed by S436, R437, V442, L453, A455, Q465, and I467 (Fig. 4*B*). Recognition of D_{-2} is mediated by a salt bridge formed between D_{-2} and R438 of SNX27. In addition to the three core residues within the DLF motif, SNX27 also recognizes upstream and downstream residues. In particularly, R438 of SNX27 forms a salt bridge with E_{-5} and one hydrogen bond with backbone carbonyl of Q_{-3}. Furthermore, side chains of Q465 and R498 of SNX27 form hydrogen bonds with the main chain oxygen of A_1 and Q_{-6}, respectively.

To validate this structure, we incorporated alanine substitutions for multiple residues within or around the DLF motif and tested their effects using GST pull-down and ITC experiments (Fig. 4 *C* and *D*). Alanine substitution of any single residue within the DLF motif completely abolished the interaction with SNX27, analogous to the triple mutation, $SNX1^{68-90}$ DLF. A systematic substitution

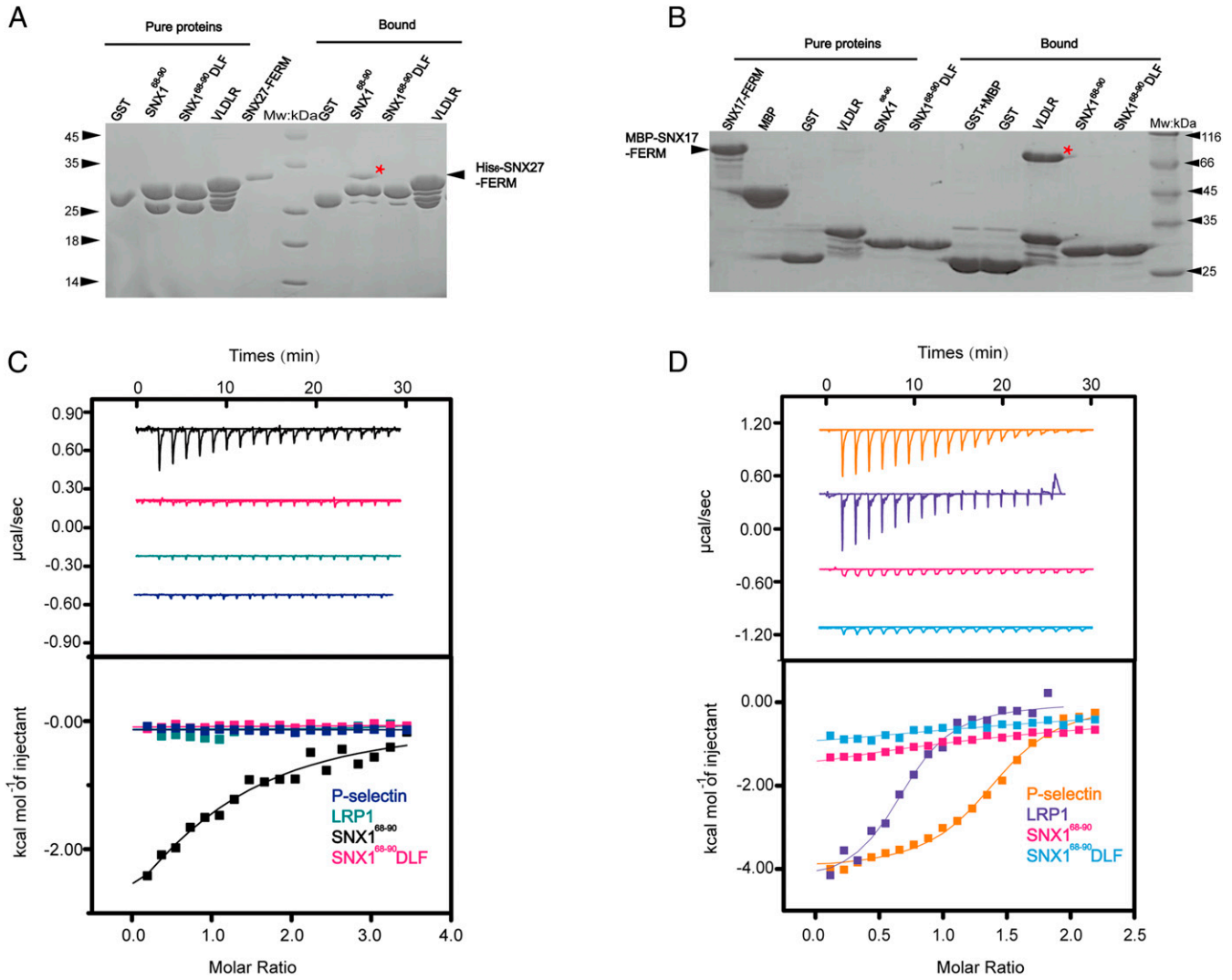

Fig. 3. The FERM domains SNX27 and SNX17 recognize the DLF and NPxY/NxxY motifs, respectively. (*A*) GST-SNX1$^{68\text{-}90}$, GST-SNX1$^{68\text{-}90}$DLF, GST-VLDLR, and GST pull-down of purified His$_6$-SNX27-FERM. Shown is a Coomassie Blue–stained SDS/PAGE gel of purified protein (*Left*) and bound samples (*Right*). * indicates the retained His$_6$-SNX27-FERM (*Left*) or MBP-SNX17-FERM (*Right*). (*B*) The GST-fusion proteins used in *A* were incubated with purified MBP-SNX17-FERM. Shown is a Coomassie Blue–stained SDS/PAGE gel of purified protein (*Left*) and bound samples (*Right*). (*C* and *D*) ITC of P-selectin, LRP1, SNX1$^{68\text{-}90}$, and SNX1$^{68\text{-}90}$ DLF titrated into MBP-SNX27-FERM (*C*) or SNX17 FL (*D*) in a buffer containing 50 mM Tris-Base pH 8.0 or 100 mM NaCl at 16 °C, respectively. Raw data are listed at the top, and integrated normalized data are listed at the bottom. Colors indicate the peptides used in the assay. Experiments were performed in triplicate, and one representative experiment is presented.

of all three residues within the DLF motif revealed 1) the −2 position of the DLF motif prefers to have a negatively charged residue (D or E); 2) the −1 position prefers to accommodate an L or I residue; and 3) most interestingly, F_0 is more strictly required, as its substitutions by other residues, including Trp (F_0W), Tyr (F_0Y), Asp (F_0D), or Leu (F_0L), all completely disrupted the association (*SI Appendix*, Fig. S5 *A–C*). Outside of the DLF motif, we found that E_{-5} also dramatically contributed to the binding to SNX27 (K_d of 20 and 144 μM for SNX1$^{68\text{-}90}$ WT and E_{-5}A, respectively). On the other hand, the alanine substitution of Q_{-3} did not significantly impair the binding. Our biochemical data are also consistent with our structural analysis as well as the sequence comparison of different DLF motifs (Fig. 1*E*). In addition to the three core residues, a negatively charged residue (D or E) dominates the −5 position. In contrast, the sequence conservation at the −3 position is poor (Fig. 1*E*).

Conversely, a number of mutations were introduced into the DLF motif-binding pocket of SNX27 (Fig. 4 *E* and *F*). R438 of SNX27 forms multiple salt bridges and hydrogen bonds with the SNX1 peptide. A reverse-charged mutant, R438E, completely abolished the binding with SNX1 in both pull-down and ITC experiments. Together with other residues, S436, R437, Q465, and I467 of SNX27 form the hydrophobic cavity to accommodate for L_{-1} and F_0 from the DLF motif. Consequently, alanine substitution of two proximate residues, SR (S436R437/AA) and QI (Q465I467/AA), markedly disrupted the interaction. On the other hand, the SR and QI mutation did not alter the binding to retromer subunit VPS26 or diacylglycerol kinase ζ (24), a soluble SNX27-binding enzyme (*SI Appendix*, Fig. S6). Finally, alanine substitution of two positively charged residues in the pocket, R438A and R498A, also reduced the binding affinity about 3~4 fold (K_d of 20, 61, and 87 μM for WT, R438A, and R498A, respectively).

Interaction between SNX1/2 and SNX27 Is Critical for Endocytic Recycling of GLUT1 and TRAILR1. SNX27, retromer, and SNX-BARs can promote endosome-to-plasma membrane recycling of many cargo proteins. Since SNX27 interacts with both retromer and SNX-BARs, we previously proposed that they form a "supercomplex"

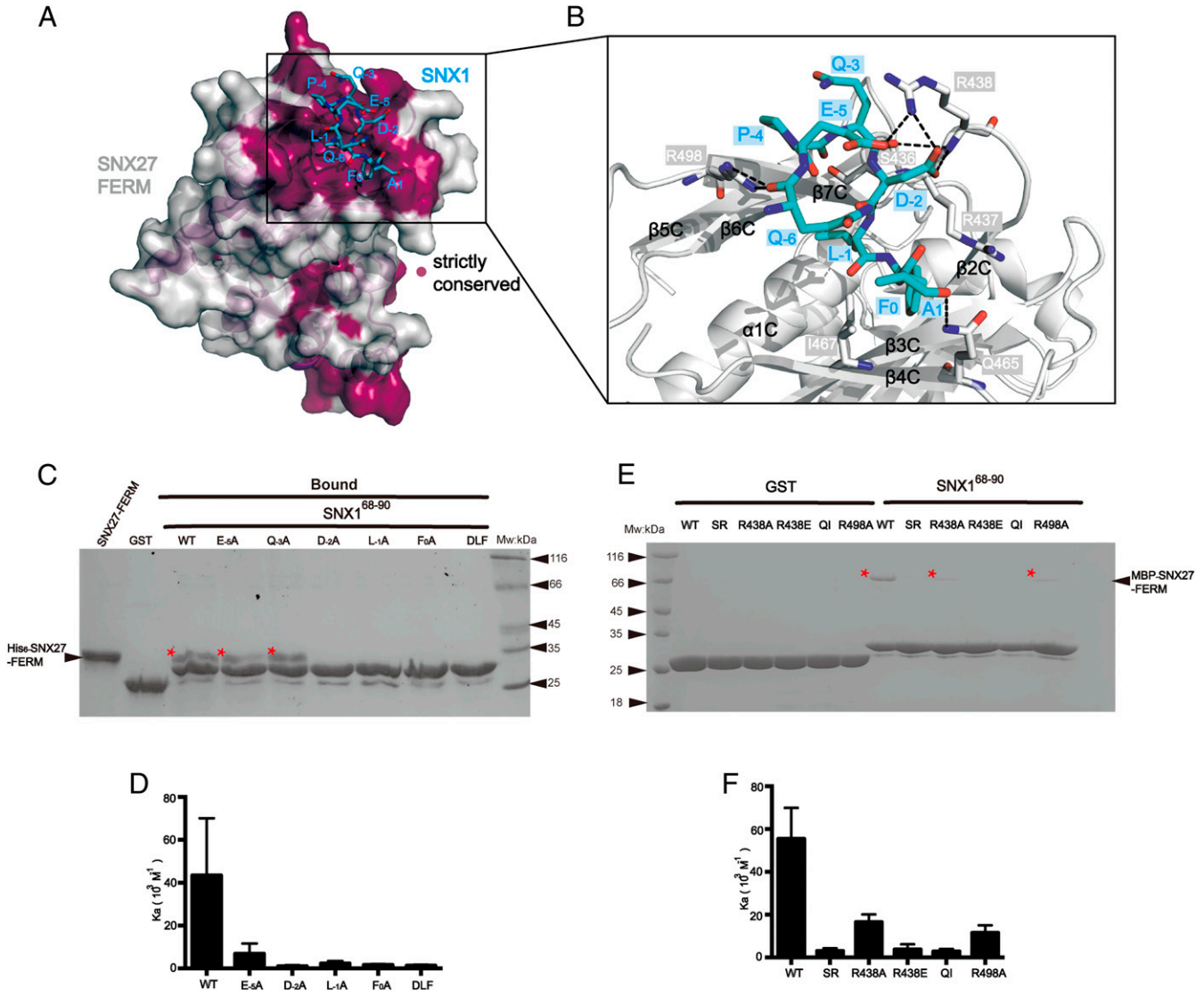

Fig. 4. Structural mechanism of recognition of the DLF motif from SNX1 by SNX27 FERM. (*A*) Conservation analysis of the FERM domain of SNX27 using the ConSurf Server (https://consurf.tau.ac.il) shows that the SNX1-binding groove among the F3 submodule is strictly conserved. The surface of SNX27-FERM is colored as light gray (nonconserved) and purple (strictly conserved). SNX1 peptide is shown in cyan sticks. (*B*) Close-up view showing the detailed binding between the SNX1 DLF motif (cyan) and SNX27-FERM (partially transparent surface; blue and red represent positive and negative charge, respectively). Critical residues on SNX27-FERM important for SNX1 recognition are highlighted in stick mode; black dashed lines indicate the observed hydrogen bonds and salt bridges in the structure. (*C*) GST, GST-SNX1$^{68\text{-}90}$ WT, and mutants ($E_{-5}A$, $Q_{-3}A$, $D_{-2}A$, $L_{-1}A$, F_0A, and DLF) pull down His_6-SNX27-FEEM. Shown is a Coomassie Blue–stained SDS/PAGE gel of bound samples of GST in right and GST-SNX1 in left. * indicates the retained His_6-SNX27-FERM. (*D*) Binding affinity between MBP-SNX27-FERM protein and WT or corresponding mutants of SNX1$^{68\text{-}90}$ peptides in *C* determined by ITC. Association constant (K_a) is shown together with errors from data fitting. (*E*) GST and GST-SNX1$^{68\text{-}90}$ pull-down of purified MBP-SNX27-FERM WT, SR, R438A, R438E, QI, and R498A, respectively. Shown is a Coomassie Blue–stained SDS/PAGE gel of bound samples of GST on the right and GST-SNX1 on the left. * indicates the retained MBP-SNX27-FERM. (*F*) Binding affinity between MBP-SNX27-FERM WT or mutants in *E* and SNX1$^{68\text{-}90}$ WT determined by ITC. Association constant (K_a) is shown together with errors from data fitting.

to promote the recycling of some cargoes (28). However, it remains undetermined whether the interaction between SNX1/2 and SNX27 is relevant for cargo recycling. We chose GLUT1 as a model cargo, which is known to be recycled in a SNX27-dependent and SNX-BAR–dependent manner (23) (Fig. 5). We generated SNX27 knockout (KO) cells using CRISPR-Cas9 technology and tested whether SNX27 WT and various SNX27 mutants, including the VPS26-binding–deficient mutant (Δ67 to Δ77), the PDZbm-binding–deficient mutant (NR, N56R58/AA), and the SNX1-binding–deficient mutants (SR, QI), could rescue the mis-sorting of GLUT1 in the SNX27 KO cell (23–25) (Fig. 5 *A*–*C*). As expected, SNX27 WT, but not the empty vector, could efficiently rescued GLUT1 mis-sorting, as assayed by the colocalization of GLUT1 and phalloidin (Fig. 5 *B* and *C*). Similar to previous studies, both the NR and the Δ67 to Δ77 mutants failed to rescue GLUT1 mis-sorting (23, 25) (Fig. 5 *B* and *C*). Furthermore, neither SR nor QI rescued GLUT1 mis-sorting, suggesting that interaction with SNX1/2 is likely required for the GLUT1-recycling function of SNX27 (Fig. 5 *B* and *C*). This observation was further supported by a surface protein biotinylation assay, which revealed that SNX27 WT, but none of the mutants, restored the surface levels of GLUT1 (Fig. 5*D* and *SI Appendix*, Fig. S7). As a control, the surface levels of integrin A5, a cargo recycled by SNX17 and retriever, was not affected by SNX27 loss (12) (Fig. 5*D* and *SI Appendix*, Fig. S7). The SNX27-SNX1/2 interaction also promoted endocytic recycling of TRAILR1, similar to GLUT1, although TRAILR1

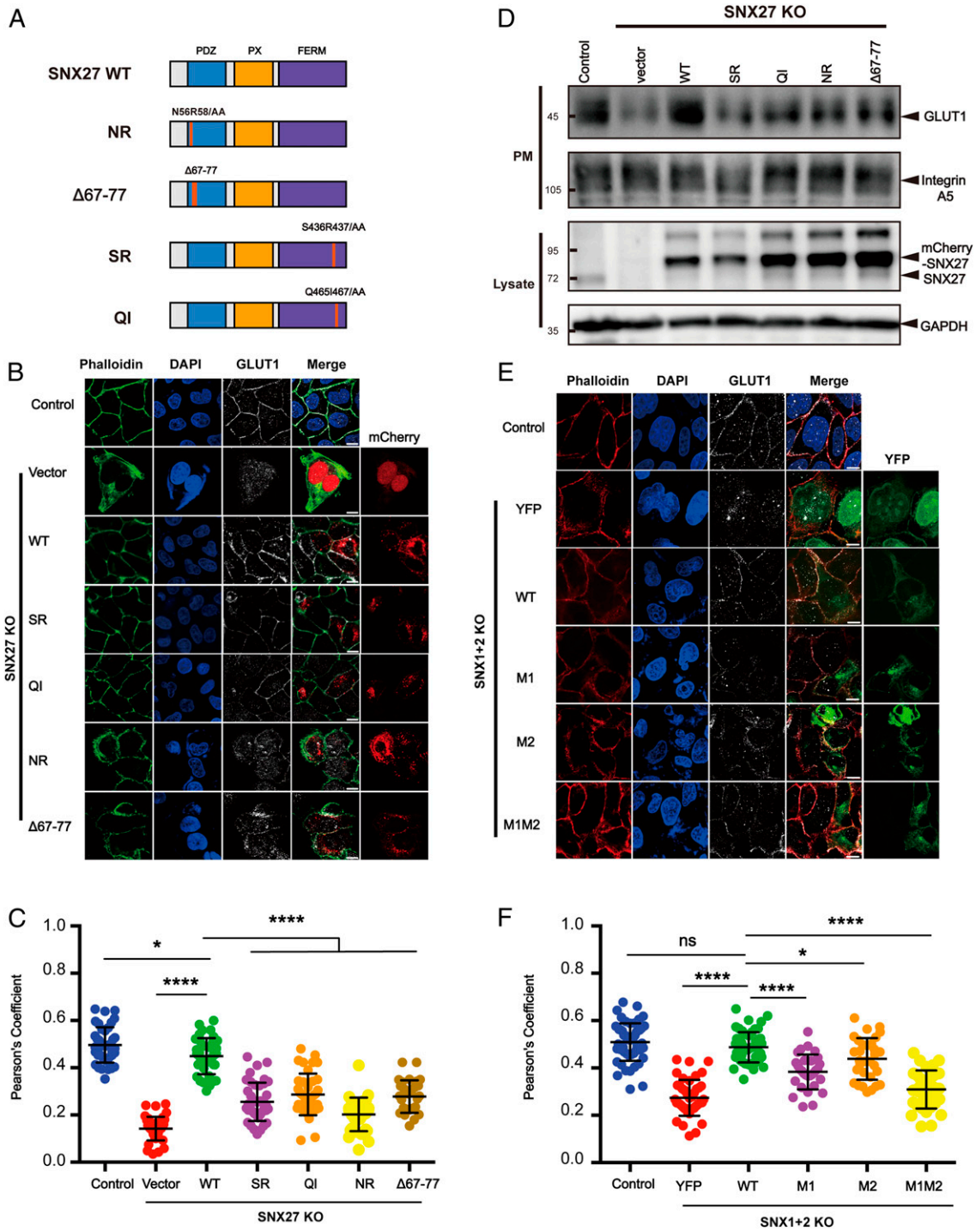

Fig. 5. The interaction between SNX27 and SNX1 is critical for endosomal recycling of GLUT1. (*A*) A schematic diagram of SNX27 constructs used in this study. (*B* and *C*) Surface distribution of GLUT1 in HeLa cell lines. The SNX27 KO cells were transfected with mCherry, mCherry-SNX27 WT, mCherry-SNX27 SR, mCherry-SNX27 QI, mCherry-SNX27 NR, and mCherry-SNX27 Δ67 to Δ77 (*Left*), while control cells were left untreated. Cells were then incubated with antibody against GLUT1 (gray) and stained with phalloidin (green). (*C*) Colocalization analysis between GLUT1 and phalloidin in *B*. Each dot represents Pearson's correlation coefficients from one cell. Data are presented as mean ± SD, and *P* values were calculated using one-way ANOVA and Tukey's multiple comparisons test. $*P < 0.05$, $0.001 < ****P < 0.0001$; figure is representative of $n = 3$ independent experiments with similar results. (*D*) Surface biotinylation level of GLUT1 and integrin A5 in HeLa cell strains. SNX27 KO cells were transfected with indicated plasmids in *A* (*Top*), while control cells were left untreated. Cells were then digested, washed, and subjected to biotin label reagent for 30 min at RT. Streptavidin agarose resin was utilized to capture biotinylated proteins. Samples were washed and used for immunoblotting (plasma membrane [PM]); mCherry-SNX27, endogenous SNX27, and GAPDH were detected in lysate. (*E* and *F*) Surface distribution of GLUT1 in HeLa cell lines. The SNX1+2 KO cells were transfected with YFP, YFP-SNX1 WT, YFP-SNX1 M1, YFP-SNX1 M2, and YFP-SNX1 M1M2 (*Left*), while control cells were left untreated. Cells were then incubated with antibody against GLUT1 (gray) and stained with phalloidin (red). (*F*) Colocalization analysis between GLUT1 and phalloidin in *D*. Each dot represents Pearson's correlation coefficients from one cell. Data were presented as mean ± SD and *P* values were calculated using one-way ANOVA and Tukey's multiple comparisons test. $*P < 0.05$, $0.001 < ****P < 0.0001$, ns, not significant; figure is representative of $n = 3$ independent experiments with similar results.

bears an SNX-BAR–binding motif, not a PDZbm (28) (*SI Appendix*, Fig. S8 *A* and *B*).

To test whether SNX1/2 interaction with SNX27 is important for cargo recycling, we generated HeLa cells that were depleted for both SNX1 and SNX2 (SNX1+2 KO) using CRISPR-Cas9 vectors simultaneously targeting SNX1 and SNX2 and performed rescue experiments (Fig. 5 *E* and *F* and *SI Appendix*, Fig. S8 *C* and *D*). Re-expression of SNX1 WT, but not the SNX27-binding–deficient mutants M1, M2, or M1M2, restored the plasma membrane localization of GLUT1 and TRAILR1, evaluated by the colocalization with phalloidin (Fig. 5 *E* and *F* and *SI Appendix*, Fig. S8 *C* and *D*). Taken together, our data suggest that the interaction between SNX1/2 and SNX27 is likely critical for endocytic recycling of many cargoes, irrespective of whether the cargo proteins are directly recognized by SNX27 or SNX-BARs.

The SNX1–SNX27 Interaction Mediates SNX27 Recruitment to Retromer in T Cells. In addition to the aforementioned cells, SNX27 also plays a critical role in polarized membrane trafficking in T cells (39). However, the mechanism by which SNX27 is recruited to PtdIns(3)P-enriched endosomes remains poorly understood. We thus tested whether the SNX1–SNX27 interaction is important for endosomal recruitment of each protein in T cells. As shown in *SI Appendix*, Fig. S9*A*, SNX1 was present as discrete puncta and colocalized with VPS35 in Jurkat T cells loaded with staphylococcal enterotoxin E superantigen, suggesting that SNX1 predominantly localizes to endosomes containing retromer complexes in T cells. When we coexpressed SNX1 WT and SNX27 WT, the majority of SNX27 was found on $SNX1^+$ puncta with little cytoplasmic distribution (Fig. 6*A*). Coexpression of SNX1 or SNX27 mutants disrupting the SNX1–SNX27 interaction did not affect puncta distribution of SNX1 in T cells. However, a larger proportion of SNX27 was found in the cytoplasm when the SNX1–SNX27 interaction was disrupted (Fig. 6 *A* and *B*). These data suggest that some proportion of SNX27 is recruited to $SNX1^+$ puncta in T cells through its interaction with SNX1. Furthermore, both SNX27 WT and PDZbm-binding mutant (NR) mainly colocalized with the retromer subunit VPS35 in APC-conjugated T cells (Fig. 6 *C* and *D*). However, when the interaction with SNX1 was disrupted in SNX27 (SR), the majority of SNX27 was distributed in the cytoplasm similar to the VPS26-binding mutant (Δ67 to 77). These data suggest that SNX27 is recruited to retromer-positive endosomes through interaction with SNX1 and VPS26.

In contrast with SNX27, both the WT and DLF motif mutant (M1M2) of SNX1 presented equivalent colocalization with VPS35 in APC-conjugated T cells regardless of the presence of superantigen (*SI Appendix*, Fig. S9 *B* and *C*). In addition, endosomal recruitment of both SNX1 and SNX27 seems to be independent of T cell receptor activation since colocalization of each protein with VPS35 was not affected by the presence of superantigen in conjugated APC (*SI Appendix*, Fig. S9*C* and Fig. 6*D*). Thus, the endosomal recruitment of SNX1 is independent of its interaction with SNX27 and could be mediated via its interaction with SNX5/6, PtdIns(3)P through the PX domain, or curved membranes via its BAR domain.

The SNX1–SNX27 Interaction Promotes Neuronal Growth and Brain Development in Zebrafish. To further define the role of the SNX27 FERM domain in vivo, we chose zebrafish as a model organism (40, 41). Zebrafish encode two SNX27 proteins (SNX27a/b) with amino acids sequence identity of 80%. Whole-mount in situ hybridization (WISH) analysis revealed that SNX27a was highly expressed in the head and spinal cord (*SI Appendix*, Fig. S10*A*), consistent with previous studies that SNX27 messenger RNA (mRNA) can be detected in the brains of mammals (34). Furthermore, semiquantitative RT-PCR uncovered continuous expression of SNX27a throughout early embryonic development (*SI Appendix*, Fig. S10*B*), which could be detected even at the one-cell stage, suggesting an important role of SNX27 in embryonic development. To address the functions of SNX27 in embryonic development, we partially depleted SNX27 using antisense morpholino oligonucleotides (MO) targeting either SNX27a or SNX27b (*SI Appendix*, Fig. S10*C*). Reduced expression of either SNX27a or SNX27b decreased the length of the CaP motor neurons by half in Tg[hb9: GFP] ml2 transgenic zebrafish, consistent with the established role of SNX27 in mammalian neuronal development (34, 42) (*SI Appendix*, Fig. S10*D*). SNX27a MO was thus selected in our following study. Remarkably, the axonal length phenotype could be largely rescued through coinjection of human full-length (FL) SNX27 mRNA, suggesting that human SNX27 can compensate for the loss of zebrafish SNX27a (Fig. 7 *A*–*C*).

To test the role of FERM domain in neuronal development, we generated an SNX27 construct deleting the FERM domain (ΔFERM) and two chimera constructs, SNX27-17 or SNX27-31, in which the SNX27 FERM domain was substituted with that of SNX17 or SNX31. These chimeric constructs are expected to retain the interaction with retromer and PDZbm-containing cargoes but lose their ability to interact with SNX1/2. Neither SNX27 ΔFERM nor the chimeras were able to restore axonal length, indicating divergent functions of FERM domains between SNX27 and SNX17/31 in vivo. Similarly, SNX27 QI and SR could not rescue the defective axonal length similar to SNX27 FL, suggesting that SNX27 association with SNX1 is important for neuronal development in zebrafish. In addition to shorter axons, we also observed that SNX27a MO led to dramatically reduced midbrains that were about 1/3 of those in the control group (Fig. 7 *D*–*F*). SNX27 FL, but none of the mutants, rescued the reduction in midbrain size (Fig. 7 *D*–*F*).

To investigate whether the interaction between SNX1 and SNX27 was critical for GLUT1 trafficking in zebrafish, we coinjected SNX27a MO together with mRNA encoding human SNX27 FL and SNX1-interacting–deficient mutants (ΔFERM, 27 to 17, 27 to 31, SR and QI). Similar to what we have observed in cultured cells, depletion of SNX27a decreased the colocalization between GLUT1 and β-catenin, a plasma membrane marker (Fig. 7*G* and *SI Appendix*, Fig. S10*E*). Importantly, SNX27 FL, but none of the mutants we tested, restored the colocalization (Fig. 7*G* and *SI Appendix*, Fig. S10*E*). Collectively, we demonstrate that the association between SNX1 and SNX27 is crucial for brain development in zebrafish, likely by regulating the trafficking of key PDZbm-containing cargoes.

Discussion

Past research has established SNX17 and SNX27, two members of the PX-FERM family, as key regulators of endocytic recycling (1, 2). Despite the conserved FERM domain, SNX17, but not SNX27, is known to mediate the transport of transmembrane proteins containing the NPxY/NxxY motif. In contrast, SNX27 mediates recycling of PDZbm-containing transmembrane proteins via its PDX domain. The underlying reason for the inability of SNX27 to regulate the trafficking of NPxY/NxxY motif-containing transmembrane proteins via its FERM domain has remained enigmatic. Here, we discover that the FERM domains of SNX17 and SNX27 have distinct functions: whereas the SNX17 FERM domain binds the NPxY/NxxY motif in cargo proteins, the SNX27 FERM domain interacts with a DLF motif found in the extended N termini of SNX1/2. The interactions are highly specific, suggesting that SNX17 and SNX27 regulate endocytic recycling through distinct mechanisms.

Our detailed structural analysis of the SNX17 and SNX27 FERM domains highlighted unique differences in the F3 module. First, a key leucine residue (L353) in the SNX17 FERM domain involved in contacting the tyrosine in the NPxY/NxxY motif is an alanine in the SNX27 FERM domain. Importantly, an SNX17 FERM domain containing an L353A mutant was unable to interact with the NPxY-containing cargo P-selectin, further supporting the importance of this residue. Moreover, using GST

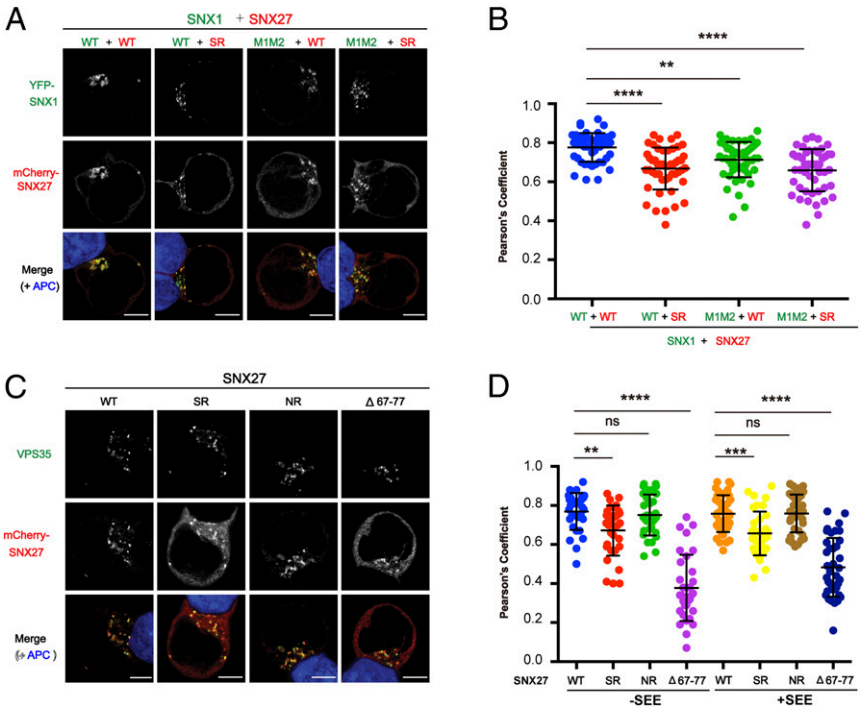

Fig. 6. Interaction with SNX1 and VPS26 mediates the endosomal recruitment of SNX27 in Jurkat T cells. Jurkat T cells were transfected with plasmids expressing YFP-SNX1 and mCherry-SNX27 (*A* and *B*) or with plasmids expressing mCherry-SNX27 (*C* and *D*) as indicated and conjugated with NALM6 B cells. (*A*) Representative images showing localization of SNX1 (green) and SNX27 (red) in T cells conjugated with staphylococcal enterotoxin E (SEE)-pulsed B cells (APC; blue). (*B*) Colocalization analysis between SNX1 and SNX27 within T cells conjugated with SEE-pulsed B cells. (*C*) Representative images showing localization of SNX27 (red) and endogenous VPS35 (green) in T cells conjugated with SEE-pulsed B cells (APC; blue). (*D*) Colocalization analysis between SNX27 and VPS35 within T cells conjugated with NALM6 B cells preloaded with or without SEE superantigen. (*A* and *C*) (Scale bar: 5 μm.) (*B* and *D*) Each dot represents a Pearson's correlation coefficient from a single conjugated T cell, and error bars indicate SD. Data shown are representative (*A* and *C*) and combined (*B* and *D*) from four (*A* and *B*) and three (*C* and *D*) independent experiments. Statistical significance was determined using one-way ANOVA with Tukey's multiple comparisons test. $^{**}P < 0.01$, $^{***}P < 0.001$, $^{****}P < 0.0001$, ns, not significant.

pull-downs and ITC, we showed that the SNX27 FERM domain was unable to interact with various NPxY/NxxY-containing cargoes, thus indicating that the SNX27 FERM domain does not interact with cargo containing these motifs. Ghai et al. previously reported that the SNX27 FERM domain could interact with the NPxY/NxxY motif, similar to the SNX17 FERM (35, 36). Our structural information, together with the biochemical and quantitative measurement of protein–protein interaction, led to a different conclusion. It should be noted that Ghai et al. based their conclusions on results from nonquantitative assays, such as peptide arrays (35). Furthermore, our results support studies from Tseng et al., who showed SNX17 and SNX31, but not SNX27, could associate with the NPxY/NxxY-containing β integrins (21).

The second key difference that we identified in the F3 module was the presence of a hydrophobic cavity surrounded by positively charged residues in the SNX27 FERM domain that was absent in the SNX17 FERM domain. We showed that this hydrophobic cavity could accommodate the DLF motif and that key amino acids within this F3 module made substantial contacts with DLF as well as with an amino acid at the −5 position, which was usually a D or E. Interestingly, the same region of SNX27 was previously shown to interact with several phosphoinositide species, including PI(3,4,5)P_3 (43). Future studies will be necessary to dissect the role of PI(3,4,5)P_3 in the SNX1–SNX27 interaction. Taken together, our biochemical and structural analyses indicate that the FERM domains of SNX27 and SNX17, while adopting a similar overall structure, have unique binding specificities (DLF or NPxY/NxxY) inferred by the presence of key conserved amino acids in the F3 module.

The mechanisms of endosomal recruitment of SNX17 and SNX27 are distinct. SNX17 is recruited to endosomes through an interaction of the retriever subunit VPS26C with a highly conserved motif found in the C-terminal tail of SNX17 (12). Mutation or deletion of this motif abrogates the interaction of SNX17 with the retriever and its endosomal recruitment and recycling of cargoes, such as $\alpha_5\beta_1$ integrin (12). On the other hand, the recruitment of SNX27 to endosomes and its ability to regulate the recycling of cargoes, such as GLUT1, relies on an interaction with the retromer subunit VPS26A via the SNX27 PDZ domain (23, 25). Herein, we show that an interaction of the SNX27 FERM domain with the DLF motif(s) found in the extended N termini of SNX1/2 also assists endosomal recruitment of SNX27 and GLUT1 recycling. This suggests that multiple interactions between SNX27 and endosomal-localized proteins contribute to its recruitment and ability to regulate the recycling of PDZbm-containing cargoes. Interestingly, mutations in SNX1 (M1, M2, and M1M2) that impact its ability to interact with SNX27 were recruited to endosomes in Jurkat T cells but still impacted GLUT1 recycling in HeLa cells, likely as a result of diminished recruitment of SNX27. The ability of the SNX1 mutants (M1, M2, M1M2) to be recruited to endosomes independent of SNX27 is likely mediated through the interaction with SNX5/6. Moreover, the individual or combined interactions of the PX domain with PI(3)P and BAR domain with curved membranes could negate any requirement for a role of SNX27 in SNX1/2 recruitment. However, despite the endosomal localization of these SNX1 mutants, the interaction with SNX27 appears obligate for GLUT1 recycling and possibly other PDZbm-containing cargoes.

Why is the interaction between SNX27 and SNX-BARs critical for GLUT1 and TRAILR1 recycling? SNX27 and SNX-BARs are

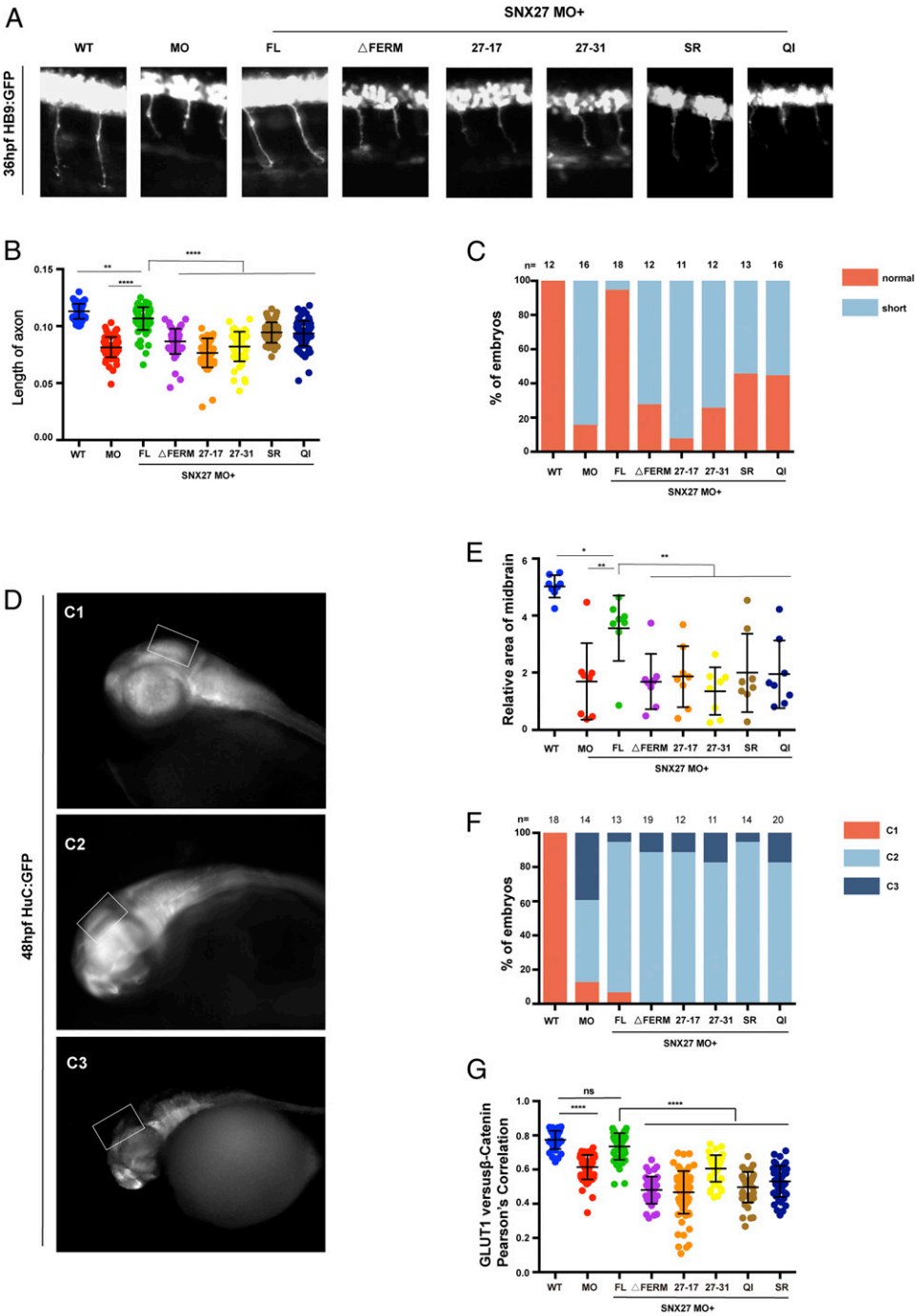

Fig. 7. The SNX1–SNX27 interaction is critical for neuronal growth and brain development in zebrafish. (*A*) Morphology of CaP axons from embryos at 36 hours postfertilization (hpf) injected with SNX27a MO and/or indicated mRNAs was determined, and representative images of at least three independent experiments were shown. All injections were performed at one-cell stage of the Tg [hb9: GFP]ml2 transgenic zebrafish embryos. (*B*) Statistical analysis of the length of CaP axons in embryos described as in *A*; each dot represents one CaP axons length in embryos, and error bars indicate the SD. The samples were measured using at least 55 axons from 11 embryos. *P* values were calculated using one-way ANOVA by Tukey's honestly significant difference (HSD) test or *t* test. ****$P < 0.0001$; ***$P < 0.001$; **$P < 0.01$. (*C*) The proportion of each class upon injection of SNX27a MO only or coinjection of indicated mRNAs is shown. All injections are performed at one-cell stage of the development. The length of the axons is divided into two grades, normal and short. Normal means the length of axon is similar to that of WT, whereas short means the length of axon is shorter than that of WT. N represents the number of embryos used for statistical analysis. (*D*) HuC expression in Tg(HuC:GFP) transgenic zebrafish. The lateral view of zebrafish midbrain at 48 hpf was divided into three levels according to the size of midbrain area. C1, normal; C2, moderate defects in midbrain; C3, severe defects in midbrain. All injections were performed at the one-cell stage of development. The white squares label the position of the midbrain. Representative images of three independent experiments were shown. (*E*) The relative area of zebrafish midbrain was measured from lateral view. Eight embryos from each group were used for analysis. Results for individual zebrafishes were plotted, and the mean and SD for each group are shown; *P* values were calculated using one-way ANOVA by Tukey's HSD test or *t* test. **$P < 0.01$; *$P < 0.1$. (*F*) The percentage of embryos in each class described in *D* and *E* are shown. N represents the numbers of embryos used for statistical analysis. *P* value was calculated using χ^2 (and Fisher's exact) test. $P < 0.0001$. (*G*) Colocalization analysis of GLUT1 with β-catenin within zebrafish. Results for individual zebrafish embryo cells are plotted, along with the mean and SD for each group. *P* values were calculated using one-way ANOVA by Tukey's HSD test or *t* test. ****$P < 0.0001$, ns, not significant.

involved in the recognition of transmembrane proteins with PDZbm and SBM, respectively. The recent cryo-electron tomography studies indicate that SNX3-retromer is sufficient to couple cargo recognition with membrane curvature generation (44). As the membrane-contacting motif is conserved between SNX3 and SNX27, SNX27-retromer may analogously facilitate the incorporation of PDZbm-containing cargoes into specific endosomal subdomains (44, 45). SNX-BARs, on the other hand, help to concentrate SBM-containing cargoes. If both SNX27-retromer and SNX-BARs promote the formation of specific endosomal subdomains, the interaction between them allows the formation of a "supercomplex" to mediate endosome-to-plasma membrane retrieval of proteins with PDZbm, SBM, or both motifs (28). The "supercomplex" model, although still rudimentary, could explain why SNX27 regulates the endocytic recycling of TRAILR1, which does not contain a PDZbm, and why SNX-BARs affect the trafficking of cargoes without SBM, such as GLUT1. In addition, the interaction between SNX27 and SNX-BARs could help endosomal recruitment of SNX27, as demonstrated by our study (Fig. 6). Additionally, we provide evidence that the interaction between SNX27 and SNX-BARs is critical for normal neuronal development in zebrafish. Overall, by identifying the unique functions of SNX17 and SNX27 FERM domains, our study provides a unified answer for many different observations in the field and lays a foundation for future discoveries concerning the physiological and pathophysiological functions of SNX family proteins.

Methods

Antibodies, reagents, and DNA constructs used in this study are presented in *SI Appendix*, Tables S2–S4, respectively. The cloning, expression, purification, and crystallization procedures for SNX27-FERM-SNX1$^{78\text{-}90}$ are provided in *SI Appendix*. X-ray diffraction data were collected at Shanghai Synchrotron Radiation facility beamline BL17U1. The data collection statistics are shown in *SI Appendix*, Table S1. Structure was solved by Se-SAD. Detailed procedures of GST pull-down and ITC experiments are given in *SI Appendix*. SNX27 and SNX1+2 KO and rescued cell lines were generated similarly to the previous study (28, 31). All zebrafish experiments were performed according to previous procedures (40, 41). More detailed information, covering that of antisense RNA probes, mRNAs, morpholino, WISH, and whole-mount immunofluorescence, is provided in *SI Appendix*.

Data Availability. Structure factor and atomic coordinates data have been deposited in Protein Data Bank (7CT1). All other study data are included in the article and/or *SI Appendix*.

ACKNOWLEDGMENTS. Research in the authors' laboratory is supported by Natural Science Foundation of China grants (91854121 and 31871429), National Key Research and Development Program of China (Grant 2018YFC1005004), Sichuan Science and Technology Program (Grant 2018RZ0128), 1.3.5 project for disciplines of excellence, West China Hospital, Sichuan University (grants ZYGD20007 and ZYJC18011 to X.M.), and a US NIH grant (DK107733 to D.D.B.).

1. P. J. Cullen, F. Steinberg, To degrade or not to degrade: Mechanisms and significance of endocytic recycling. *Nat. Rev. Mol. Cell Biol.* **19**, 679–696 (2018).
2. J. Wang *et al.*, Endosomal receptor trafficking: Retromer and beyond. *Traffic* **19**, 578–590 (2018).
3. C. Burd, P. J. Cullen, Retromer: A master conductor of endosome sorting. *Cold Spring Harb. Perspect. Biol.* **6**, a016774 (2014).
4. K. J. McMillan, H. C. Korswagen, P. J. Cullen, The emerging role of retromer in neuroprotection. *Curr. Opin. Cell Biol.* **47**, 72–82 (2017).
5. S. A. Small, G. A. Petsko, Retromer in Alzheimer disease, Parkinson disease and other neurological disorders. *Nat. Rev. Neurosci.* **16**, 126–132 (2015).
6. Y. Tu, L. Zhao, D. D. Billadeau, D. Jia, Endosome-to-TGN trafficking: Organelle-vesicle and organelle-organelle interactions. *Front. Cell Dev. Biol.* **8**, 163 (2020).
7. N. Personnic, K. Bärlocher, I. Finsel, H. Hilbi, Subversion of retrograde trafficking by translocated pathogen effectors. *Trends Microbiol.* **24**, 450–462 (2016).
8. Z. Daniloski *et al.*, Identification of required host factors for SARS-CoV-2 infection in human cells. *Cell* **184**, 92–105.e16 (2020).
9. P. Zhang, G. Monteiro da Silva, C. Deatherage, C. Burd, D. DiMaio, Cell-penetrating peptide mediates intracellular membrane passage of human papillomavirus L2 protein to trigger retrograde trafficking. *Cell* **174**, 1465–1476.e13 (2018).
10. X. Yong *et al.*, Targeting endosomal recycling pathways by bacterial and viral pathogens. *Front. Cell Dev. Biol.* **9**, 648024 (2021).
11. S. Weeratunga, B. Paul, B. M. Collins, Recognising the signals for endosomal trafficking. *Curr. Opin. Cell Biol.* **65**, 17–27 (2020).
12. K. E. McNally *et al.*, Retriever is a multiprotein complex for retromer-independent endosomal cargo recycling. *Nat. Cell Biol.* **19**, 1214–1225 (2017).
13. E. Derivery *et al.*, The Arp2/3 activator WASH controls the fission of endosomes through a large multiprotein complex. *Dev. Cell* **17**, 712–723 (2009).
14. T. S. Gomez, D. D. Billadeau, A FAM21-containing WASH complex regulates retromer-dependent sorting. *Dev. Cell* **17**, 699–711 (2009).
15. D. Jia *et al.*, WASH and WAVE actin regulators of the Wiskott-Aldrich syndrome protein (WASP) family are controlled by analogous structurally related complexes. *Proc. Natl. Acad. Sci. U.S.A.* **107**, 10442–10447 (2010).
16. A. Singla *et al.*, Endosomal PI(3)P regulation by the COMMD/CCDC22/CCDC93 (CCC) complex controls membrane protein recycling. *Nat. Commun.* **10**, 4271 (2019).
17. C. A. Phillips-Krawczak *et al.*, COMMD1 is linked to the WASH complex and regulates endosomal trafficking of the copper transporter ATP7A. *Mol. Biol. Cell* **26**, 91–103 (2015).
18. R. T. Böttcher *et al.*, Sorting nexin 17 prevents lysosomal degradation of β1 integrins by binding to the β1-integrin tail. *Nat. Cell Biol.* **14**, 584–592 (2012).
19. W. Stockinger *et al.*, The PX-domain protein SNX17 interacts with members of the LDL receptor family and modulates endocytosis of the LDL receptor. *EMBO J.* **21**, 4259–4267 (2002).
20. F. Steinberg, K. J. Heesom, M. D. Bass, P. J. Cullen, SNX17 protects integrins from degradation by sorting between lysosomal and recycling pathways. *J. Cell Biol.* **197**, 219–230 (2012).
21. H. Y. Tseng *et al.*, Sorting nexin 31 binds multiple β integrin cytoplasmic domains and regulates β1 integrin surface levels and stability. *J. Mol. Biol.* **426**, 3180–3194 (2014).
22. P. Temkin *et al.*, SNX27 mediates retromer tubule entry and endosome-to-plasma membrane trafficking of signalling receptors. *Nat. Cell Biol.* **13**, 715–721 (2011).
23. F. Steinberg *et al.*, A global analysis of SNX27-retromer assembly and cargo specificity reveals a function in glucose and metal ion transport. *Nat. Cell Biol.* **15**, 461–471 (2013).
24. T. Clairfeuille *et al.*, A molecular code for endosomal recycling of phosphorylated cargos by the SNX27-retromer complex. *Nat. Struct. Mol. Biol.* **23**, 921–932 (2016).
25. M. Gallon *et al.*, A unique PDZ domain and arrestin-like fold interaction reveals mechanistic details of endocytic recycling by SNX27-retromer. *Proc. Natl. Acad. Sci. U.S.A.* **111**, E3604–E3613 (2014).
26. D. Jia, T. S. Gomez, D. D. Billadeau, M. K. Rosen, Multiple repeat elements within the FAM21 tail link the WASH actin regulatory complex to the retromer. *Mol. Biol. Cell* **23**, 2352–2361 (2012).
27. M. E. Harbour, S. Y. Breusegem, M. N. Seaman, Recruitment of the endosomal WASH complex is mediated by the extended 'tail' of Fam21 binding to the retromer protein Vps35. *Biochem. J.* **442**, 209–220 (2012).
28. X. Yong *et al.*, Mechanism of cargo recognition by retromer-linked SNX-BAR proteins. *PLoS Biol.* **18**, e3000631 (2020).
29. B. Simonetti *et al.*, Molecular identification of a BAR domain-containing coat complex for endosomal recycling of transmembrane proteins. *Nat. Cell Biol.* **21**, 1219–1233 (2019).
30. O. Kovtun *et al.*, Structure of the membrane-assembled retromer coat determined by cryo-electron tomography. *Nature* **561**, 561–564 (2018).
31. L. Mao *et al.*, Phosphorylation of SNX27 by MAPK11/14 links cellular stress-signaling pathways with endocytic recycling. *J. Cell Biol.* **220**, e202010048 (2021).
32. H. Zhang *et al.*, The retromer complex and sorting nexins in neurodegenerative diseases. *Front. Aging Neurosci.* **10**, 79 (2018).
33. J. Lee *et al.*, Adaptor protein sorting nexin 17 regulates amyloid precursor protein trafficking and processing in the early endosomes. *J. Biol. Chem.* **283**, 11501–11508 (2008).
34. X. Wang *et al.*, Loss of sorting nexin 27 contributes to excitatory synaptic dysfunction by modulating glutamate receptor recycling in Down's syndrome. *Nat. Med.* **19**, 473–480 (2013).
35. R. Ghai *et al.*, Structural basis for endosomal trafficking of diverse transmembrane cargos by PX-FERM proteins. *Proc. Natl. Acad. Sci. U.S.A.* **110**, E643–E652 (2013).
36. R. Ghai *et al.*, Phox homology band 4.1/ezrin/radixin/moesin-like proteins function as molecular scaffolds that interact with cargo receptors and Ras GTPases. *Proc. Natl. Acad. Sci. U.S.A.* **108**, 7763–7768 (2011).
37. J. J. Burden, X. M. Sun, A. B. García, A. K. Soutar, Sorting motifs in the intracellular domain of the low density lipoprotein receptor interact with a novel domain of sorting nexin-17. *J. Biol. Chem.* **279**, 16237–16245 (2004).
38. E. Krissinel, K. Henrick, Inference of macromolecular assemblies from crystalline state. *J. Mol. Biol.* **372**, 774–797 (2007).
39. N. González-Mancha, I. Mérida, Interplay between SNX27 and DAG metabolism in the control of trafficking and signaling at the IS. *Int. J. Mol. Sci.* **21**, E4254 (2020).
40. D. Liu *et al.*, Structure of TBC1D23 N-terminus reveals a novel role for rhodanese domain. *PLoS Biol.* **18**, e3000746 (2020).
41. J. Qin *et al.*, Structural and mechanistic insights into secretagogin-mediated exocytosis. *Proc. Natl. Acad. Sci. U.S.A.* **117**, 6559–6570 (2020).
42. V. Arkhipova *et al.*, Characterization and regulation of the hb9/mnx1 beta-cell progenitor specific enhancer in zebrafish. *Dev. Biol.* **365**, 290–302 (2012).
43. R. Ghai *et al.*, Phosphoinositide binding by the SNX27 FERM domain regulates its localization at the immune synapse of activated T-cells. *J. Cell Sci.* **128**, 553–565 (2015).
44. N. Leneva, O. Kovtun, D. R. Morado, J. A. G. Briggs, D. J. Owen, Architecture and mechanism of metazoan retromer:SNX3 tubular coat assembly. *Sci. Adv.* **7**, eabf8598 (2021).
45. X. Yong, D. D. Billadeau, D. Jia, All ways lead to Rome: Assembly of retromer on membranes with different sorting nexins. *Signal Transduct. Target. Ther.* **6**, 139 (2021).